Local density augmentation and dynamic properties of hydrogen-and non-hydrogen-bonded supercritical fluids: A molecular dynamics study

Ioannis Skarmoutsos and Jannis Samios[a)]
Laboratory of Physical Chemistry, Department of Chemistry, University of Athens, Panepistimiopolis 157-71, Athens, Greece

(Received 11 July 2006; accepted 13 December 2006; published online 25 January 2007)

The local density inhomogeneities in neat supercritical fluids were investigated via canonical molecular dynamics simulations. The selected systems under investigation were the polar and hydrogen-bonded fluid methanol as well as the quadrupolar non-hydrogen-bonded carbon dioxide one. Effective local densities, local density augmentation, and enhancement factors were calculated at state points along an isotherm close to the critical temperature of each system ($T_r=1.03$). The results obtained reveal strong influence of the polarity and hydrogen bonding upon the intensity of the local density augmentation. It is found that this effect is sufficiently larger in the case of the polar and associated methanol in comparison to those predicted for carbon dioxide. For both fluids the local density augmentation values are maximized in the bulk density region near $0.7\rho_c$, a result that is in agreement with experiment. In addition, the local density dynamics of each fluid were investigated in terms of the appropriate time correlation functions. The behavior of these functions reveals that the bulk density dependence of the local density reorganization times is very sensitive to the specific intermolecular interactions and to the size of the local region. Also, the estimated local density reorganization time as a function of bulk density of each fluid was further analyzed and successfully related to two different time-scale relaxation mechanisms. Finally, the results obtained indicate a possible relationship between the single-molecule reorientational dynamics and the local density reorganization ones. © *2007 American Institute of Physics*. [DOI: 10.1063/1.2431370]

I. INTRODUCTION

It is well known that supercritical fluids (scfs) exhibit solvent properties which may be varied from gaslike to liquidlike values with small changes in pressure or temperature. Due to this particular behavior, the dissolving power of scfs could be adjusted by slightly varying the thermodynamic parameters, tuning by this way selectively the solubility of different solute types in these fluids. These features make scfs attractive alternatives to liquid solvents for several chemical applications. For this reason, numerous studies have been devoted so far to explore the physicochemical properties and specifically the local structure of some widely used sc solvents.

As a result of this effort, the origin of this peculiar behavior of scfs has been attributed to noticeable density inhomogeneities occurring in such systems. In other words, the microscopic picture of a scf in its compressible regime resembles that of an inhomogeneous molecular system with low- and high-density regions. Moreover, experimental results have led to the conclusion that density inhomogeneities in scfs may be distinguished into the local and long-range order ones. In a recent review,[1] the author pointed out that the origins of these distinct density inhomogeneity effects are different. Note, for instance, that the bulk density dependence of the density inhomogeneity in both cases is not in general the same. Specifically, it was found that local density inhomogeneities (LDIs) are maximized at bulk densities in the range from $1/3\rho_c$ to $1/2\rho_c$ while for isotherms close to the critical point the long-range ones are at the critical density ρ_c.[1–6] Generally, the excess of solvent molecules around a solute molecule may be positive (local density augmentation) or negative (depletion). Undoubtedly, the knowledge of the characteristic way in which the average local density enhancement varies as a function of the bulk solvent density at a constant temperature T, greater than the critical one, T_c, is of particular importance for the quantitative understanding of the phenomenon. Despite the research effort on the field over the past decades, however, many interesting questions are still subject to debate.

To the authors' knowledge, systematic studies devoted to the short-range LDI of neat scfs have been not so much up to now. On the other hand, studies on dilute sc solutions have shown that the short-range environment of a solute molecule can in general differ from that of a solvent one. In the case of attractive solutes diluted in sc solvents, spectroscopic studies show average local density enhancement that is two to five times the bulk one.[7–12] Results have been also obtained from computer simulations (CSs) employed to model dilute solutions near the critical point.[7,12–18] According to the recent literature on the field, the local density augmentation in some nonpolar neat scfs, such as methane, ethane, CO_2, and C_6F_6, has been investigated by a number of authors using vibra-

[a)]Author to whom correspondence should be addressed. Electronic mail: isamios@chem.uoa.gr

tional spectroscopy.[19–22] The results obtained have shown that also in that case the average local density around a solvent molecule is greater than the bulk one. Note that the estimated magnitude of the density augmentation is found to be sufficiently smaller in comparison to the former case of a solute.

On the other hand, there are only a limited number of CS studies devoted to the estimation of the local density augmentation of nonpolar neat scfs that have been reported up to now.[5,7,16,23,24] Generally, the very small local density augmentation observed experimentally and theoretically in nonpolar neat fluids compared to nonpolar dilute fluid solutions has been attributed to the different asymmetry strength of the solute-solvent and solvent-solvent intermolecular forces.

To further this research interest and in the case of polar as well as hydrogen-bonded (HB) neat scfs, Saitow *et al.* carried out recent experiments of neat sc fluoroform[25–27] (CHF_3) and methanol (MeOH).[28] In the case of CHF_3 and along the isotherm $T=1.02T_c$, they estimated local densities around a molecule which were approximately equal to a factor of 2 larger compared to the bulk values at low densities. This suggestion has been reexamined by Song and Maroncelli[23] in a more recent molecular dynamics (MD) CS treatment. The results obtained have shown that (a) the extent of the local density augmentation simulated in both scfs is sufficiently smaller than the experimental values and (b) the local density augmentation in CHF_3 exceeds that of ethane due to the electrostatic character of the interactions present in the former fluid. It appears, however, that the difference between the simulated values of this property for both fluids is very small. The authors in that study have systematically examined the disagreement between simulation and experiment in the case of sc CHF_3. According to their considerations, the reason for this discrepancy could be the assumption of a linear proportionality to the local density of an observable quantity made as well as the methodology employed to derive local densities from the Raman shifts observed by Saitow *et al.*[26] As mentioned above, Saitow and Sasaki[28] published new results on the local density augmentation of sc MeOH as a function of the bulk density and reduced temperature $T_r=T/T_c=1.02$ (522.9 K) based on the spontaneous Raman spectra of the C–O stretching mode of the molecule. The local density augmentation of sc MeOH obtained in that study is evaluated by a direct comparison to the values corresponding to sc CHF_3 and ethane.[23] As a result, it is found that the local density augmentation of the sc MeOH is more pronounced than those observed for simple non-HB fluids. Additionally, the local density augmentation of sc MeOH was estimated in that study by a second method and on the basis of previously published NMR data,[29] performed at the same temperature. Finally, they pointed out that the amounts of the local density augmentation of sc MeOH estimated by two different experimental techniques exhibit a similar extent (further information for the experimental techniques employed to investigate LDIs are given in Sec. II A).

As a main conclusion, from all the aforementioned studies on dilute sc solutions and neat scfs, it has been recognized that among the parameters on which the local density augmentation effect is expected to depend strongly is certainly the relative strengths of the solute-solvent and solvent-solvent intermolecular forces in a scf. However, a deeper and quantitative understanding of the aforementioned dependence has not yet been achieved and remains a particular problem still open.

The present work is closely related to this important factor by investigating systematically the local density augmentation effect in pure scfs using the MD simulation technique. Concretely, given the above inconsistencies between experimental and theoretical results on the local density augmentation in neat scfs, it would seem very useful to study further this subject in order to increase our quantitative understanding of these phenomena. Thus, due to the complete lack of any CS and integral equation—theoretical study on sc MeOH devoted exclusively to the problem of the LDI in the system so far, we decided to study this fluid further and to examine the suggestion made by the authors in Ref. 28. Additionally, we have investigated the quadrupolar sc CO_2 fluid at the same reduced temperature, and bulk densities and the corresponding results obtained have been contrasted to those of sc MeOH.

Finally, our CS methodology used and the results obtained for both fluids are presented and discussed in the following sections.

II. FUNDAMENTALS

A. Local density inhomogeneities: Search methodology

In this section, we will present the methodology employed in our study to estimate the properties under investigation as well as, briefly, the most usual spectroscopic techniques used by several researchers to monitor the mean local density of a fluid around the molecules.

In the framework of a pure theoretical (integral equation) as well as a CS treatment, the appropriate quantity required to monitor the average local density of a fluid is the corresponding center of mass (c.o.m.) pair distribution function (PDF) $g_{\mathrm{com}}(r)$. It is due to the fact that local densities are usually defined in terms of the average number of particles (coordination number N_{co}) found in the first solvation shell of a particle, given by the following relation:

$$N_{\mathrm{co}}(\rho,R_c)=4\pi\rho\int_0^{R_c} g_{\mathrm{com}}(r)r^2dr. \tag{1}$$

The quantity ρ denotes the bulk number density of the fluid at a given thermodynamic state point and R_c the cutoff distance that specify the volume of the solvation shell of a particle.

Specifically, if one wants to estimate the excess local density in the near critical regime of a fluid, it is more convenient to calculate first of all the well-known *effective* local density $\rho_{\mathrm{eff},l}$ according to the relation

$$\rho_{\mathrm{eff},l}(\rho) = \frac{N_{\mathrm{co}}(\rho)}{N_{\mathrm{co}}(\rho_{\mathrm{ref}})}\rho_{\mathrm{ref}}. \quad (2)$$

The employed values of the reference density ρ_{ref} correspond to liquidlike ones typically in the range between $2\rho_c$-and $3\rho_c$.[7] We used this methodology here, originally used by Maroncelli and co-workers in recent works.[7,23] Moreover, the cutoff distance R_c depends on the reference density used and is determined as the position of the first minimum of the corresponding c.o.m. PDF observed at this high density. The cutoff distance selected in this way is employed in the present simulations carried out at bulk densities of interest.

According to the literature,[7,23] to describe how far the local density exceeds in comparison to the bulk one, we use the excess local density (*augmentation*) relative to the bulk, $\Delta\rho_{\mathrm{eff},l}=\rho_{\mathrm{eff},l}-\rho$, or the well-known *enhancement* factor $F_{\mathrm{enh}}=\rho_{\mathrm{eff},l}/\rho$. The maximum value $\Delta\rho_{\mathrm{eff},l}(\mathrm{max})$ observed at a given density of the fluid provides a measure of the extent of the local density augmentation.

Besides the static local density augmentation effects, it is of particular interest to study the behavior of the time dependent distribution of the local density around the molecules in the sample. Knowledge about the relative time scales concerning the single-molecule dynamics and those of the local density redistribution around it is of particular importance for the investigation of whether the dynamics of an arbitrary molecule will be affected by the full time dependent redistribution of the local density around it.

In a recent CS treatment of a two-dimensional (2D) Lennard-Jones (LJ) pure monatomic fluid, Maddox *et al.*[30] studied the time scale for the local solvent reorganization (density redistribution), which may affect the dynamics of an arbitrary solvent molecule. In that study the authors defined the instantaneous local density deviation $\Delta\rho_l(t)$ relative to the mean local one as $\Delta\rho_l(t)=\rho_l(t)-\langle\rho_l\rangle$, and calculated the dynamics of this quantity in terms of its autocorrelation function (acf),

$$C_{\Delta\rho_l}(t) = \frac{\langle\Delta\rho_l(0)\cdot\Delta\rho_l(t)\rangle}{\langle[\Delta\rho_l(0)]^2\rangle}. \quad (3)$$

The property of interest here is the correlation time, $\tau_{\Delta\rho_l}$.

$$\tau_{\Delta\rho_l} = \int_0^\infty C_{\Delta\rho_l}(t)dt. \quad (4)$$

The time $\tau_{\Delta\rho_l}$ corresponds to the local density reorganization time, in other words to the time on which the local density around an arbitrary solvent changes.

In this CS study, the local density redistribution time as a function of ρ, $\tau_{\Delta\rho_l}(\rho)$, has been obtained on the basis of the aforementioned methodology. In addition, we have investigated the dependence of $C_{\Delta\rho_l}(t)$ and $\tau_{\Delta\rho_l}(\rho)$ on the size of the local region around a molecule by increasing the cutoff distance R_c.

From experimental point of view, the determination of effective local densities is usually detected indirectly by measuring spectroscopically some particle (solute or solvent)-centered observable quantity that is sensitive to the properties of the short-range local solvents (local density) around it. The most often employed spectroscopic techniques in such studies have been systematically reviewed.[1] For additional details, the reader is also referred to a more recent publication.[7] According to these studies and in the case of a solute diluted in a scf, the evidence as well as the estimation of an enhancement of the local density in comparison to the bulk one may be deduced from the solvatochromic shift observed in UV-visible spectroscopy for electronic transitions along an isotherm near the critical one. Note, however, that vibration relaxation or dephasing rate techniques are also powerful tools to provide evidence of the aforementioned phenomenon through a proper selection of the normal vibrational mode as the observable quantity. Other techniques that have been already used in experimental studies of LDIs are the far infrared (FIR) absorption and in one case also[28] the NMR spectroscopy.[29] As far as we know, Raman[19,21,22,26–28,31] and FIR (Ref. 25) investigations have been reported for a few pure scfs focused on the behavior of the mean local density around a particle at a given isotherm as a function of the bulk density. As pointed out by several workers on the field, however, in order to predict local densities in this way one must know how the observable property depends on the solvent conditions. For this purpose, one uses the behavior of the observable quantity more often calibrated in solvents at liquid densities. The basic reason for this consideration is that the macroscopic and local properties in liquid solvents are almost identical. It is useful to note here that in any case the local density obtained from experiment may be accurate if the exact relation among the observable quantity and density is known. However, the exact "functional" form of this connection is usually unknown and only approximate expressions may be used for this purpose.

B. Computational details

All simulations were carried out at thermodynamic conditions for which experimental data are available from the literature. Both fluids were simulated in the *NVT* ensemble at the same reduced temperature $T_r=T/T_c=1.03$, which for sc MeOH ($T_c=512.6$ K) corresponds to 527 K and for sc CO_2 ($T_c=304.6$ K) to 313 K. For each fluid we performed nine *NVT*-MD simulations for a series of densities in the range of $0.2\rho_c-2.0\rho_c$. Note that one supplementary MD run of sc MeOH was carried out at a density of $0.95\rho_c$ and at the same temperature. The simulated state points are presented in Table I.

The simulations were carried out with 500 molecules in the simulation box using standard periodic boundary conditions. To check the reliability of the results obtained, we carried out trial runs with larger system sizes. Thus, it is found that the estimated properties corresponding to systems with 864 molecules were converged to those of 500 ones. Note that in order to achieve equilibrium of the fluids at each state point of interest, the corresponding simulation was extended to at least 350 ps followed by at least 500 ps trajectory over which the structural and dynamic properties were calculated. In all simulations the integration time step was 1 fs. The equations of motion were integrated using a leapfrog-type Verlet algorithm. Note that the thermostat of

TABLE I. The simulated densities at $T/T_c=1.03$ ($T_c=304.13$ K and $T_c=512.60$ K) for sc CO_2 and MeOH. The coordination numbers $N_{co}(\rho,R_c)$, corresponding to a cutoff distance R_c equal to the distance of the first coordination shell at the density $\rho=2\rho_c$, are also presented for each system.

Thermodynamic state points		Coordination numbers $N_{co}(\rho,R_c)$[a]	
Index	ρ/ρ_c[b]	sc CO_2	sc MeOH
A	0.1903	1.285	1.363
B	0.3529	2.306	2.458
C	0.6095	3.830	3.937
D	0.8597	5.174	5.167
E	1.1441	6.621	6.465
F	1.2660	7.230	6.981
G	1.4329	8.058	7.694
H	1.5654	8.714	8.280
I	2.0000	10.964	10.248

[a]For CO_2 $R_c=0.60$ nm and for MeOH $R_c=0.63$ nm.
[b]For CO_2, $\rho_c=0.4676$ g/cm^3, and for MeOH, $\rho_c=0.2720$ g/cm^3.

Berendsen *et al.* with a temperature relaxation of 0.5 fs was also used.[32] In addition, the intramolecular geometry of the species was constrained by using the SHAKE method.[33] In the case of CO_2, the SHAKE method has been employed in an appropriate way to ensure the linearity and rigidity of the molecule.[34,35]

The intermolecular interactions are represented as pairwise additive with site-site LJ plus Coulomb electrostatic interactions due the quadrupole moment of CO_2 and the dipole moment of MeOH molecules. For unlike interaction sites, the Lorentz-Berthelot combining rules were used. The elementary physical potential model EPM2 was used to describe the site-site interactions of CO_2 (Ref. 36) whereas the OPLS-UA one was used for MeOH.[37] Note that these models have been used in earlier successful simulations of both neat systems at liquid and sc conditions[38–42] as well as in CS studies of MeOH in sc CO_2,[43] water-CO_2 interface,[44] and other binary sc mixtures.[45]

We used a cutoff radius of 1.2 nm for all LJ interactions, and long-range corrections have been also taken into account. Moreover, to account for the long-range electrostatic interactions we used the Ewald summation technique based on the more exact approximation of the Newton-Gregory forward difference interpolation scheme.[34,35]

III. RESULTS AND DISCUSSION

A. Local structure density augmentation

1. sc CO_2

In the case of sc CO_2 we have calculated the radial PDFs between the interaction sites of different molecules as a function of density and at nine thermodynamic state points (A–I). The study of the local intermolecular structure of the fluid is based on the c.o.m. PDFs. A more detailed analysis of the structural results obtained for the C–O and O–O PDFs is not crucial for this study and for this reason is not presented hereafter.

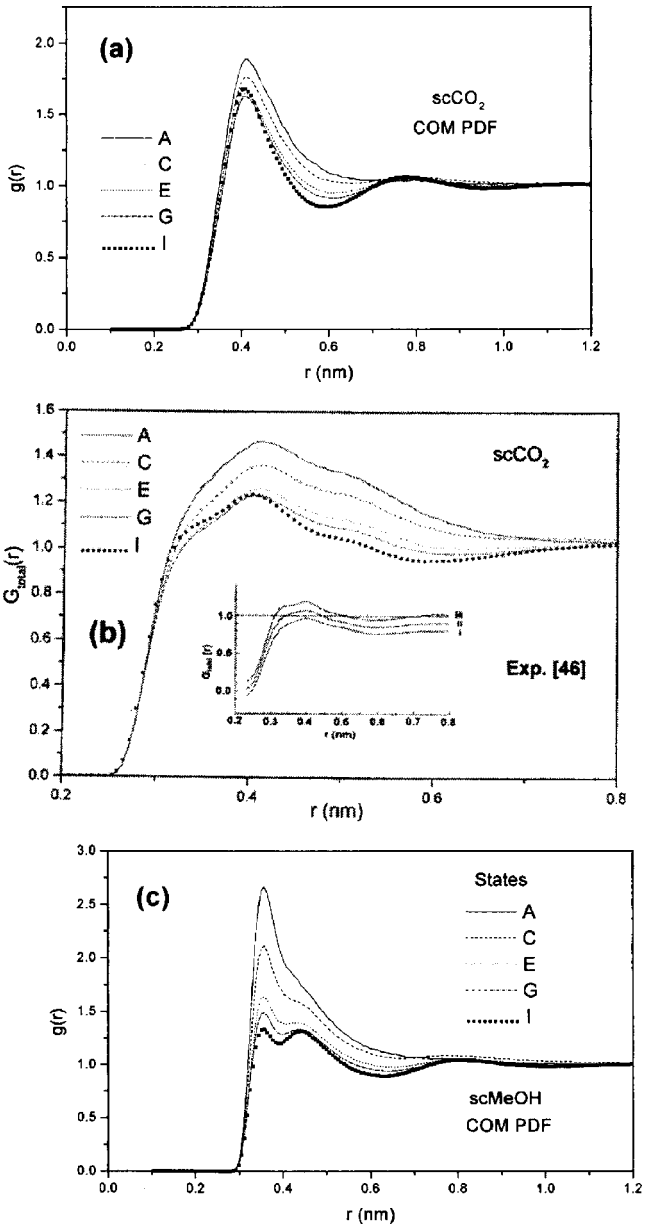

FIG. 1. (a) c.m. radial PDFs of sc CO_2. (b) The calculated neutron weighted total radial PDFs of sc CO_2, in comparison with the experimental ones (Ref. 46) measured at bulk densities $1.781\rho_c$ (i), $2.015\rho_c$ (ii), and $2.187\rho_c$ (iii) (inset figure). (c) c.m. radial PDFs of sc MeOH.

The C–C c.o.m. PDFs at the selected state points A, C, E, G, and I are shown in Fig. 1(a). From the comparison of these functions, it is seen that they exhibit a first peak localized at a distance of 4.09 Å for state A with a marginal shift to 4.15 Å at the highest system density studied (state I).

In contrast to the first peak positions, we may also observe a density dependence of the first peak intensity at constant temperature as expected. Concretely, the intensity of this function decreases from the value 1.89 (state A) to 1.62 (state I). Furthermore, the first peak is followed by a distinct minimum and further by a strongly reduced second maximum, while in all cases the third peak is not apparent. The first minimum increases on going from the lowest system density (state A) to the highest one (state I). The position of the first minimum of this function at state point I is observed

at 6.0 Å and, according to the method employed to calculate local densities, this distance has been taken into account in our local density calculations as the cutoff one at each bulk density of the fluid under study.

Up to now several sets of measurements of the intermolecular structure of sc CO_2 at various isotherms have been reported. Among these studies we mention that of Chappini *et al.*[46] who reported neutron diffraction (ND) experiments on sc CO_2 along three sc isotherms (T=313, 373, and 473 K). Specifically, their ND measurements at 313 K (T_r =1.03) were carried out at three densities in the high-density region, namely, at $\rho=1.781\rho_c$, $2.015\rho_c$, and $2.187\rho_c$. Since the state point $(T_r,\rho)=(1.03,2.015\rho_c)$ studied by ND is almost identical to the simulated state I, it is feasible to compare the results obtained from both techniques. Thus we decided to compare the total intermolecular atom-atom radial PDFs, $G_{\text{total}}(r)$, which is calculated as the weighted sum of the O–O, C–C, and C–O partial site-site radial PDFs according to the relation[46]

$$G_{\text{total}}(r) = 0.403g_{\text{O–O}}(r) + 0.133g_{\text{C–C}}(r) + 0.464g_{\text{C–O}}(r). \tag{5}$$

The $G_{\text{total}}(r)$ obtained at state points A, C, E, G, and I are shown in Fig. 1(b). From the comparison of these PDFs we see that they exhibit characteristic first maxima around the distance of 4.1 Å that is quite close to the position of the first maximum in C–C PDFs. The intensity of the first peaks appears to be strongly reduced by increasing the system density. In addition, the short-range part (up to 3.8 Å) of these PDFs exhibits a well formed shoulder which is more pronounced at the highest density studied (state I). The formation of this shoulder is due to the contribution of the first maximum of the O–O and C–O PDFs, which are located at shorter distances compared to those of the c.m. PDFs. Finally, on the basis of these results and the ND weighted PDFs for different densities [shown in Fig. 6 of Ref. 46 and also as inset in Fig. 1(b) of this work], we may observe a good agreement between experiment and simulation.

Of great interest for our study is the behavior of the average coordination numbers, $N_{\text{co}}(\rho,R_c)$, obtained for the first coordination shell of a particle up to the distance R_c as a function of density ρ and at constant temperature. The numbers $N_{\text{co}}(\rho,R_c)$ are presented in Table I. In addition, Fig. 2(a) depicts $N_{\text{co}}(\rho,R_c)$ vs ρ/ρ_c along the isotherm T_r=1.03. From Fig. 1(a) we may observe that N_{co} is clearly nonlinear density dependent, indicating the presence of a local density augmentation around an arbitrary particle in the neat fluid. In view of the above, we have estimated the excess local density at different densities of the fluid using the well-established methodology described in Sec. II A, and the results are shown in Fig. 2(b). Concretely, Fig. 2(b) shows the values of the "local density augmentation," $\Delta\rho_{\text{eff},l}$, divided by ρ_c in the region up to the first and second solvation shells of the molecules in sc CO_2. The corresponding results for the local density enhancement F_{enh} are presented in Fig. 2(c). The smooth curves through the points in Fig. 2(b) represent the best fits of the simulated data to the four-parameter a, b, c, and ρ_0 often proposed Weibull line shape function[7,47]

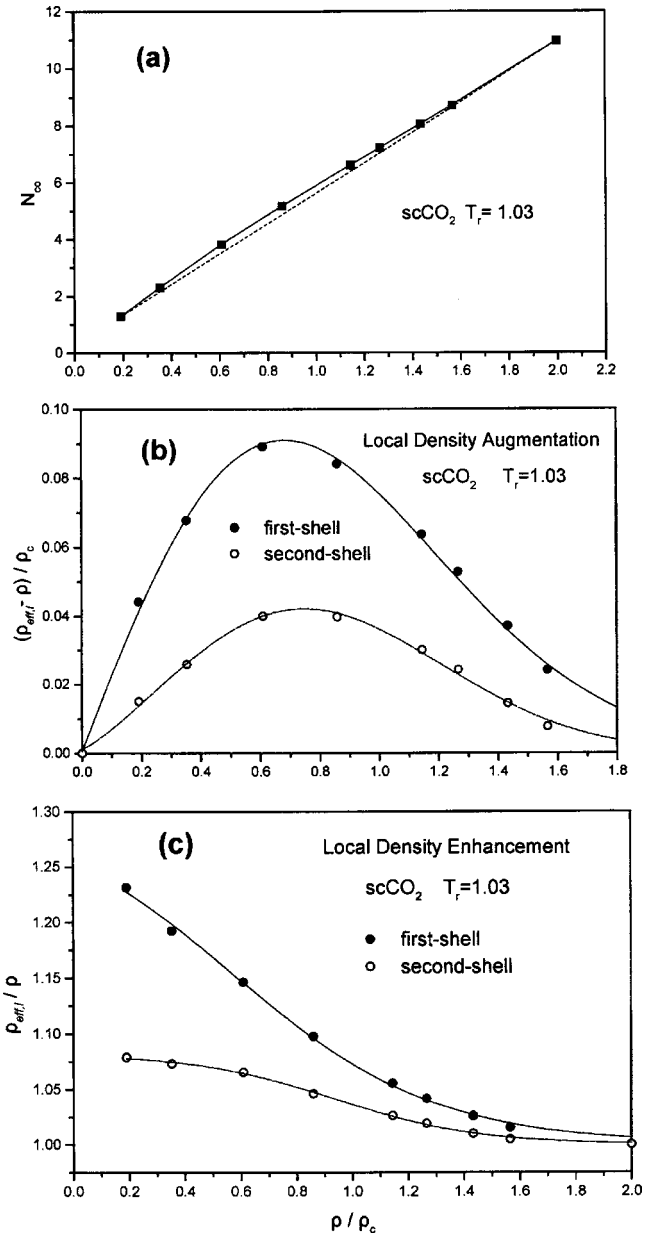

FIG. 2. The density dependence of (a) the coordination number for the first solvation shell of sc CO_2. (b) The calculated local density augmentation values for the first and second shells of sc CO_2 and (c) the calculated local density enhancement factors for the first and second shells of sc CO_2.

$$\Delta\rho_{\text{eff},l} = a\left(\frac{c-1}{c}\right)^{(1-c)/c}\left[\frac{\rho-\rho_0}{b}+\left(\frac{c-1}{c}\right)^{1/c}\right]^{c-1} \times\exp\left\{-\left[\frac{\rho-\rho_0}{b}+\left(\frac{c-1}{c}\right)^{1/c}\right]^{c}+\frac{c-1}{c}\right\}. \tag{6}$$

The maximum value for $\Delta\rho_{\text{eff},l}$ obtained from this fit represents the measure of the extent of the local density augmentation. In the case of F_{enh}, the curves through the points in Fig. 2(c) represent the best fits of the simulated data to a model function. As mentioned in Ref. 7, in most cases an exponential function of the type $F_{\text{enh}}(\rho)=1+a\exp(-b\rho)$ fits the data quite accurately. However, in the framework of the present treatment the data sets F_{enh}, for both neat fluids up to the first and second shells we have examined, cannot be reasonably fitted to the former function. We have found through

TABLE II. The fitted parameters of the Weibull and sigmoidal Boltzmann functions, corresponding to local density augmentation and enhancement factors for a cutoff distance equal to the distance R_c of the first and second shell of CO_2 and MeOH.

Weibull parameters	sc CO_2		sc MeOH	
	First shell	Second shell[a]	First shell	Second shell[a]
a	0.091	0.042	0.163	0.067
b/ρ_c	0.974	0.994	0.986	0.967
c	1.989	2.322	1.957	2.104
ρ_0/ρ_c	0.683	0.748	0.683	0.723
Sigmoidal Boltzmann parameters	sc CO_2		sc MeOH	
	First shell	Second shell	First shell	Second shell
a'	1.309	1.082	1.517	1.136
b'/ρ_c	0.368	0.255	0.354	0.260
ρ_0'/ρ_c	0.566	0.940	0.626	0.925

[a]For the second of CO_2 R_c=0.95 nm and for MeOH R_c=1.01 nm.

trial fits of several model functions that a function of the sigmoidal Boltzmann type, $F_{enh}(\rho)=1+((a'-1)/[1+\exp((\rho-\rho_0')/b')])$, might be proposed as the most suitable one for the fit of these data. The values of all parameters obtained from the fits performed in this study are presented in Table II.

As can be seen from Fig. 2(b), the effective local densities are augmented above ρ for densities smaller than $1.6\rho_c$. The maximum value of $\Delta\rho_{eff,l}=0.091\rho_c$ in the first shell is observed at $0.68\rho_c$. In the case of the second shell this maximum value is $\Delta\rho_{eff,l}=0.042\rho_c$ and is observed at $0.75\rho_c$. In other words, in the case of the second shell, the maximum value of the local density augmentation is about half of that one obtained for the first shell. Moreover, it is quite similar to the value found in a previous MD study on solvatochromic shifts in sc CO_2 at $T=1.05T_c$ (Fig. 8, Ref. 47). From Fig. 2(c), by increasing the density of the fluid we observe a decrease in F_{enh} for the first shell from the gas-phase limit $(\rho_{eff,l}/\rho)_0=1.255$, which as mentioned above follows a sigmoidal Boltzmann behavior with density. When the effective local density in the second shell of molecules is considered, both the corresponding maximum $\Delta\rho_{eff,l}$ and limit $(\rho_{eff,l}/\rho)_0$ values decrease as expected. Note finally that the comparison of the MD predictions for $\Delta\rho_{eff,l}$ or F_{enh} of neat sc CO_2 with results from suitable experiments is impossible due to the lack of such experimental information up to now. It should be mentioned, however, that Nakayama *et al.*[21] studied the density dependence of the Raman spectra for CO_2 along six isotherms in the temperature range $0.96\leqslant T/T_c\leqslant 1.06$ and densities in the region $0<\rho/\rho_c<2.0$. The Raman spectra were taken in the low-wave-number domain (>100 cm^{-1}) as well as in the frequency domain of the $2\nu_2$ bending vibrational band. According to the concluding remarks in that study, the density dependence of the corresponding $2\nu_2$ spectra obtained led the authors to assume that the molecules in sc CO_2 "make aggregates with an enhanced local density," which to the best of our knowledge has not been determined quantitatively from the aforementioned and other subsequent experimental data so far.

2. sc MeOH

As in the case of sc CO_2, the radial PDFs between all the interaction sites as well as the c.o.m. PDF of different MeOH molecules were calculated as functions of density and at $T_r=1.03$. Note that due to the geometry of a MeOH molecule in the ground state its c.o.m. does not coincide with the nucleus position of any atom on it. Therefore, the c.o.m. PDF of such a fluid may not be obtained experimentally in general and the only source of information are careful computer simulation studies.

Due to the importance of the c.m. PDFs in this study, we present and discuss the behavior of these functions as well as results for $\Delta\rho_{eff,l}$ and F_{enh}, obtained for sc MeOH. To our knowledge, due to the lack of simulated and integral equation–theoretical results of this kind, no systematic comparison between theoretical and spectroscopic experimental $\Delta\rho_{eff,l}$ and F_{enh} data for sc MeOH has been reported so far. Therefore, it becomes feasible to compare our CS results for $\Delta\rho_{eff,l}$ with experiment. A representative comparison between the c.o.m. PDFs of sc MeOH corresponding to the state points A, C, E, G, and I is illustrated in Fig. 1(c). This figure shows how the amplitude and the shape of the main peaks in these PDFs vary with density in the range $0.19\leqslant\rho/\rho_c\leqslant 2.0$. Note that the short-range part ($r\leqslant 5$ Å) of these functions consists of two overlapping peaks the amplitude of which is density dependent. It is seen that the first peak of them at about 3.5 Å becomes sharper and higher than the second one as the density decreases at constant temperature. On the basis of the behavior of these PDFs, we may conclude that over the density range investigated, sc MeOH remains highly structured at relatively short intermolecular distances. Finally, concerning the behavior of the simulated site-site PDFs of the fluid with density (not shown here), we have to mention that they provide the well-known characteristics of HB systems presented and discussed also in previous MD simulation studies of this fluid at comparable sc conditions.[41]

Let us now focus on the behavior of $N_{co}(\rho,R_c)$ obtained for the first shell of sc MeOH, presented in Table I and Fig. 3(a). From these results, we may observe that the deviation of $N_{co}(\rho,R_c)$ from a linear dependence with density is greater here in comparison with sc CO_2. This result obviously indicates a quite stronger average local density augmentation around the methanol particles in comparison with sc CO_2.

The estimated excess local density $\Delta\rho_{eff,l}/\rho_c$ as a function of the bulk one, for the first and second shells of MeOH molecules, is depicted in Fig. 3(b). The corresponding results for $F_{enh}=\rho_{eff,l}/\rho$ are presented in Fig. 3(c). The smooth curves in Fig. 3(b) represent the best fits of the Weibull line shape function to the simulated data, whereas the dotted curves in Fig. 3(c) denote the fitted sigmoidal Boltzmann function. As can be seen from Fig. 3(b), the effective local densities are augmented above ρ for densities smaller than $1.6\rho_c$. The maximum value of $\Delta\rho_{eff,l}=0.163\rho_c$ obtained for the first shell is observed at $\rho=0.68\rho_c$, while for the second one with $\Delta\rho_{eff,l}=0.067\rho_c$ at $\rho=0.72\rho_c$.

Interestingly, it is found that the $\Delta\rho_{eff,l}/\rho_c$ values for the HB associated fluid MeOH are about two times greater than those obtained for the nonpolar and nonassociated fluid CO_2.

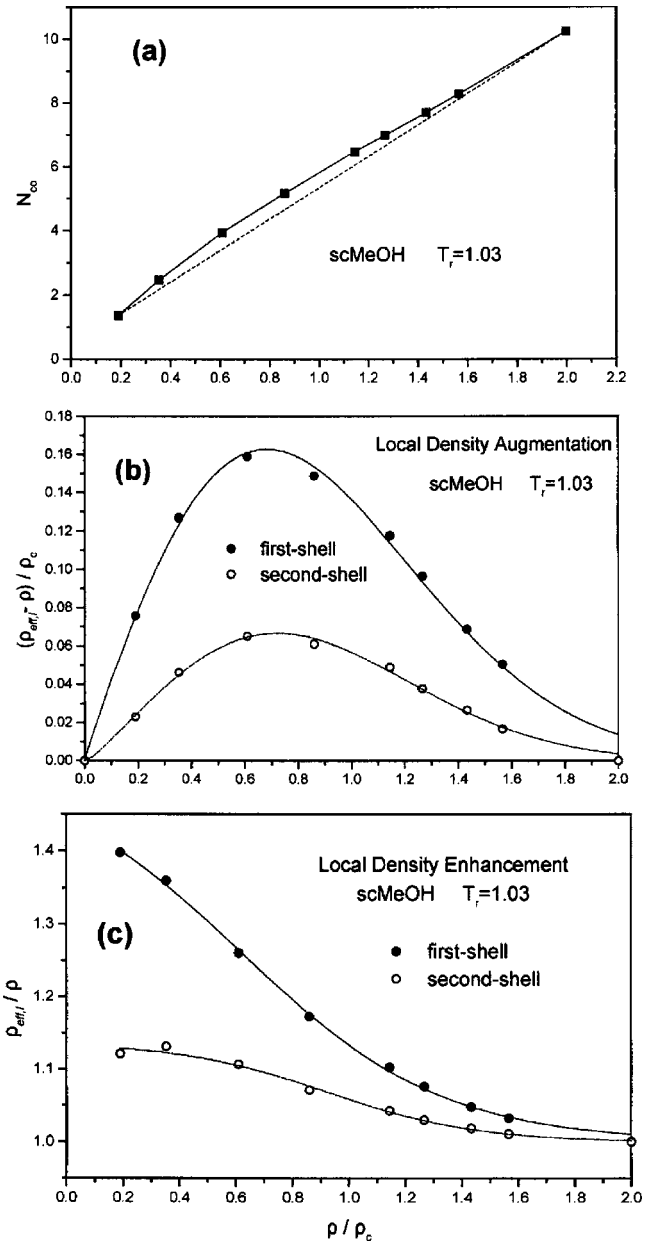

FIG. 3. Same as in Fig. 2, but for sc MeOH.

This observation might be explained in terms of the existence of the HB network, which is present not only in liquid but also in sc MeOH and has been investigated by our group in a previous study[41] at comparable conditions. This fact contributes additionally to the formation of energetically more stable clusters in sc MeOH, creating in this way a more connective local molecular network in comparison with the non-HB CO_2 fluid.

The values of F_{enh} for the first and second shells are presented in Fig. 3(c). By increasing the density, we clearly see a decrease in F_{enh} for the first shell from the gas-phase limit $(\rho_{eff,l}/\rho)_0=1.442$, which in this case provides also a sigmoidal Boltzmann behavior with density. For the second shell, both the corresponding maximum $\Delta\rho_{eff,l}$ and zero density limit $(\rho_{eff,l}/\rho)_0$ values are smaller than in the case of the first shell.

As mentioned in the Introduction, Saitow and Sasaki[28] reported also experimental results concerning the density dependence of the local density augmentation in sc MeOH. According to their data, the local density augmentation in sc MeOH is more pronounced than those observed for simple non-HB fluids. However, as in the case of the MD investigations of sc CHF_3 by Song and Maronecelli,[23] our MD results for sc MeOH indicate similarly a sufficiently smaller degree of local density augmentation in comparison with experiment.

Therefore, it is very important to notice herein some possible reasons, which in the case of the experimental investigations could result to different estimations of the local densities. The first reason has been already mentioned and is related to the methodology employed for the analysis of the density dependence of the spectral shifts obtained from experimental studies. The second one is the dependence of the local density augmentation value estimated on the basis of spectroscopic measurements of a selected vibrational mode of the molecules in the fluid.

Taking this consideration into account, in a more recent study Saitow *et al.*[27] estimated the local density augmentation in sc CHF_3 by measuring the spontaneous Raman spectra of the C–F symmetric stretch ν_2 and the $C-F_3$ symmetric deforming ν_3 modes. By analyzing separately the results obtained from each vibrational mode measurement, the estimated local densities are sufficiently smaller in the case of the ν_3 mode. Furthermore, in that study when the authors analyzed their spectral shifts by the Onsager reaction field method, the estimated local densities were even smaller than in the previous case (see Figs. 10 and 11 in Ref. 27). In the case of the ν_3 mode, the latter results were very close to the simulation values obtained by Song and Maroncelli.[23] The authors in Ref. 27 tried to interpret this behavior by assuming that the vibrational motion becomes strongly affected by the dielectric structure as the correlation length of density fluctuations is larger than the radius of the first solvation shell of CHF_3, making thus the ν_2 mode more sensitive than the ν_3 one to the dielectric environment in the vicinity of a vibrating molecule.

However, this mode sensitivity has not been taken into consideration in the Raman spectroscopic investigation of sc MeOH,[28] where Saitow and Sasaki reported the results obtained from the shifts of one specific vibrational mode (C–O stretch). This treatment, together with the assumption of linear density dependence of the spectral shifts and widths, might be a possible reason for the deviation between our simulation and experiment. In a HB associated fluid such as MeOH, where the local density augmentation effects are more pronounced, the nonlinearities are expected to be greater. This suggestion has been also supported by Saitow *et al.*[27] Concretely, we have to note that in a spectroscopic investigation of the local environments in scfs, one has to be very careful in selecting as probe the appropriate vibrational mode and the methodology employed to analyze spectral shifts.

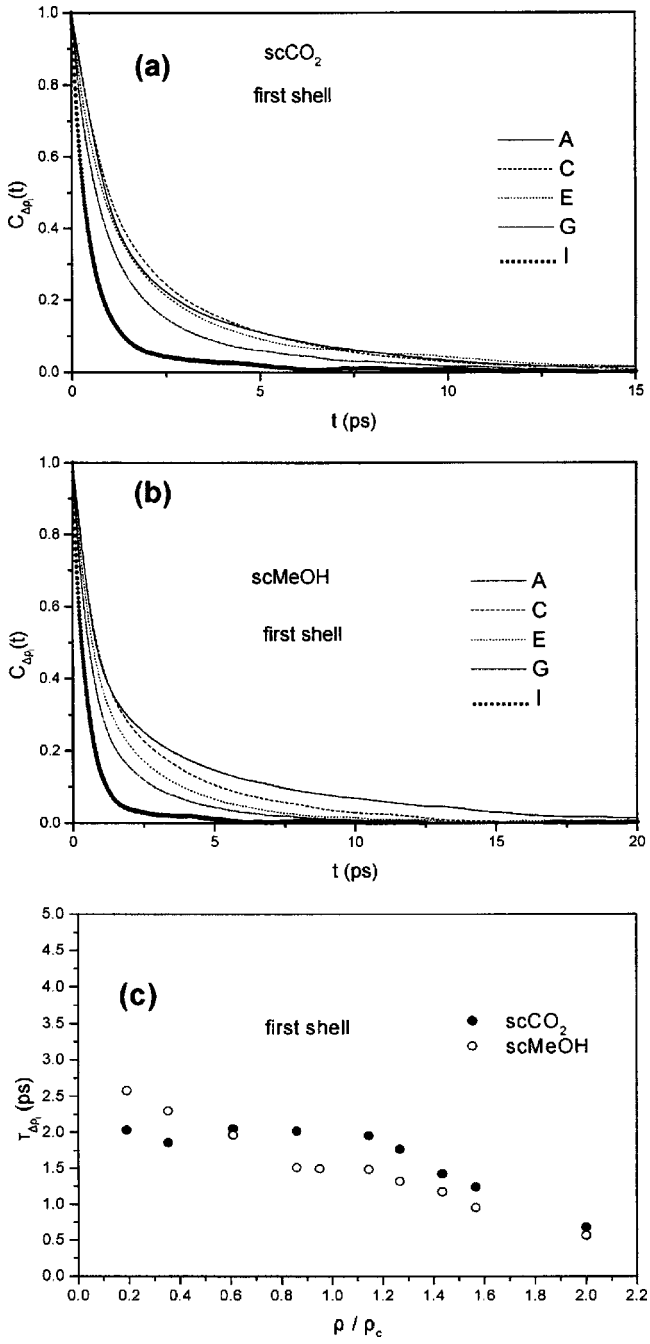

FIG. 4. (a) The calculated local density acfs $C_{\Delta\rho_l}(t)$ for the first shell of molecules in sc CO_2 at state points A, C, E, G, and I. (b) Same as in (a) but for the first shell of sc MeOH. (c) The density dependence of the corresponding correlation times $\tau_{\Delta\rho_l}$ for the first shell of sc CO_2 and sc MeOH.

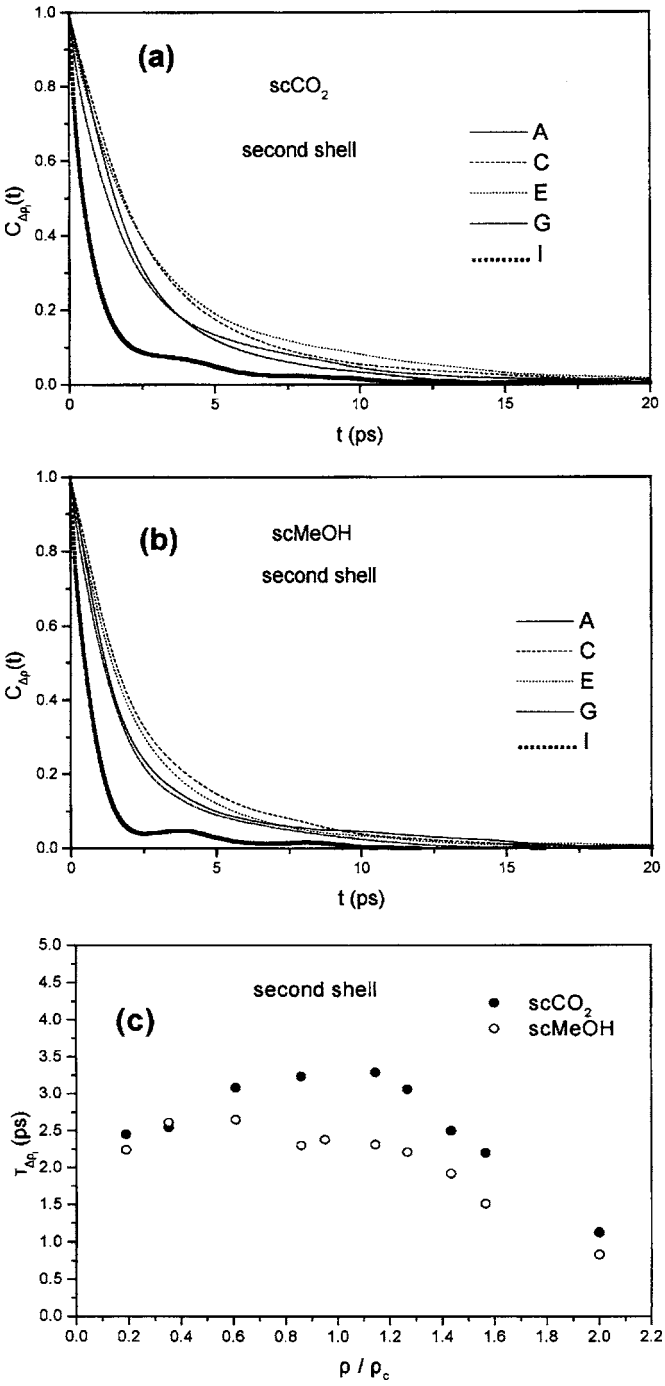

FIG. 5. As in Fig. 4 but for the second shell of sc CO_2 and sc MeOH.

B. Local density dynamics

1. *sc* CO_2

As mentioned above, by analyzing the acf $C_{\Delta\rho_l}(t)$ it is possible to determine the local environment lifetimes $\tau_{\Delta\rho_l}$ of the species in a fluid at each thermodynamic state point under investigation.

The acfs $C_{\Delta\rho_l}(t)$ of sc CO_2 are displayed in Figs. 4(a) and 5(a). By investigating the density dependence of these functions, we may observe that the time required of them to approach zero decreases with increasing density (from state A to I). Note also that at each investigated state point the time required for $C_{\Delta\rho_l}(t)$ to approach zero is larger for the second shell in comparison with the first one. Thus, we may conclude that the shape of these acfs changes significantly from low to high densities for both shells, signifying in this way the density effect upon the dynamics of the local environment around each molecule.

As pointed out in Ref. 30, the acf $C_{\Delta\rho_l}(t)$ obtained for a 2D model of monatomic LJ fluids cannot be fitted with single exponential-type decay functions. A similar behavior has been also observed for sc CO_2 in this study, where the time evolution of $C_{\Delta\rho_l}(t)$ obtained for the first shell indicates the existence of two different time-scale relaxation mecha-

nisms. Yet, we found that these two local density reorganization relaxation mechanisms are more apparent in the low-density region.

However, to explore this in a quantitative manner, we attempted to describe the shape of $C_{\Delta\rho_l}(t)$ for the first shell by means of several fitting function models. We have found through trial fits of several models that a function consisting of two separate contributions might be proposed as the most appropriate one to interpret these data. The best results were obtained with the following functional form:

$$C_{\Delta\rho_l}(t) = C_1(t) + C_2(t) = ce^{-t/t_1} + (1-c)e^{-t/t_2}. \quad (7)$$

This fact confirms the beliefs that the description of the dynamical behavior of the local environment around each molecule in a scf involves two relaxation processes, namely, one responsible for the short-time dynamics and the other describing the long-time behavior.

In the case of the second coordination shell, the shape of $C_{\Delta\rho_l}(t)$ could not be well fitted with the aforementioned model function, especially in the high-density region. This indicates presumably that the mechanisms responsible for the relaxation of the local environment around a tagged molecule become more complicated, as the length scale of the cutoff radius defining the coordination shell increases.

Results from the aforementioned procedure for the first shell are presented in Fig. 6, where the analysis of $C_{\Delta\rho_l}(t)$ in two components for some representative state points, corresponding to the low, intermediate and high-density region (states A, E, and I), is depicted. The parameter values c, t_1, and t_2 obtained from the fit of the model function at each investigated state point are summarized in Table III.

By inspecting carefully the curves in Fig. 6 and the data in Table III, we may easily conclude that, more or less, each of the components $C_1(t)$ and $C_2(t)$ contributes to the formation of $C_{\Delta\rho_l}(t)$ in the whole investigated density range. The difference, however, between the zero-time amplitudes and the decay times to zero of these two distinct correlations is quite remarkable. Note also that by increasing the bulk density, especially in the density range $1.2-2.0\rho_c$, both acfs decay to zero faster.

More precisely, the acf $C_1(t)$ contributes mainly to the shape of $C_{\Delta\rho_l}(t)$ at very short time scales and decays to zero quite fast, while $C_2(t)$ at larger time scales and decays to zero quite slower in comparison with $C_1(t)$. From this behavior, we may conclude that the proposed function reveals the contribution of a relatively fast relaxation mechanism and a slower one in the time dependent local density reorganization. In other words, the relaxation of the first shell local environment around each particle in the fluid is a two time-scale dynamical process.

Concerning the zero-time amplitudes $C_1(0)$ and $C_2(0)$, we see that in the whole density range the values of $C_1(0)$ are significantly larger than the corresponding $C_2(0)$ ones. Moreover, in the high-density region the values of $C_1(0)$ increase with increasing density, while the values of $C_2(0)$ exhibit an opposite behavior. This finding indicates that the contribution of the slow relaxation process in the local environment reorganization mechanism weakens at higher densities.

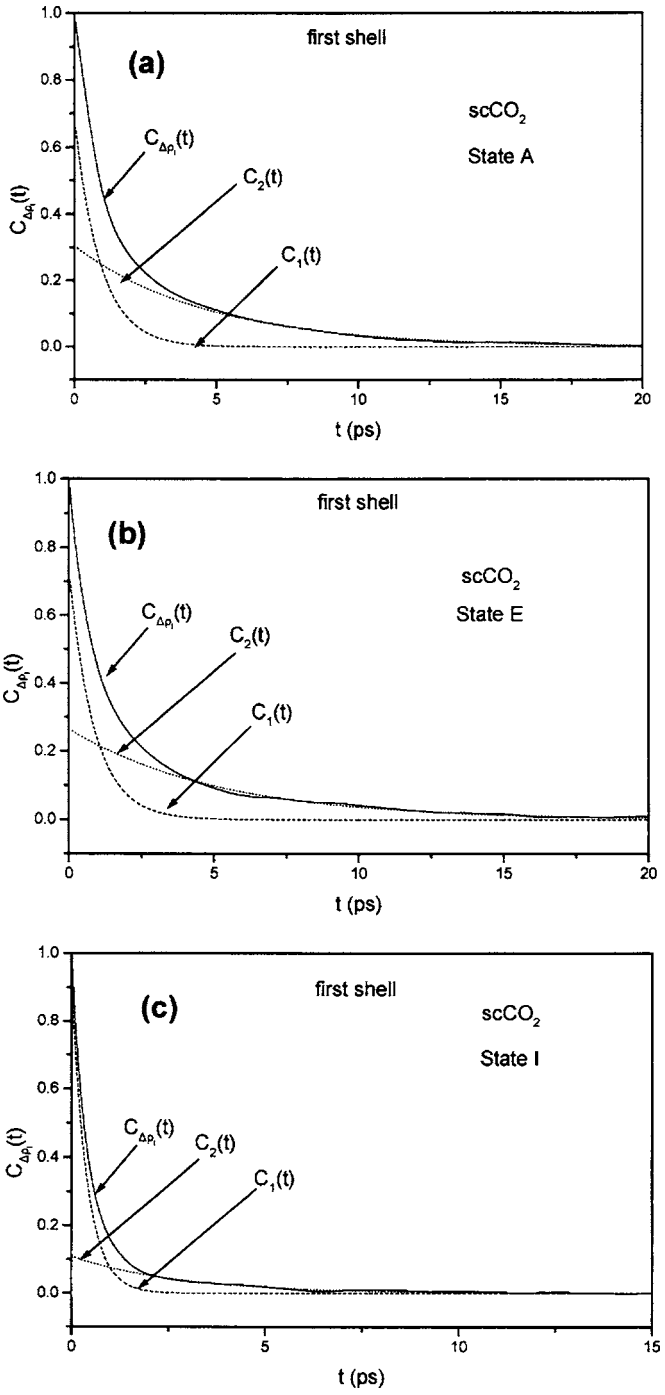

FIG. 6. Analysis of the calculated total local density acfs $C_{\Delta\rho_l}(t)$ for the first shell of molecules in sc CO_2 in two components $C_1(t)$ and $C_2(t)$ for some representative (a) low, (b) intermediate, and (c) liquidlike bulk densities.

In the following paragraphs we will present and discuss the correlation times $\tau_{\Delta\rho_l}$ corresponding to acfs $C_{\Delta\rho_l}(t)$. The correlation times $\tau_{\Delta\rho_l}$ for both coordination shells are plotted against density in Figs. 4(c) and 5(c), and summarized in Table IV. We easily see from these data that the times $\tau_{\Delta\rho_l}$ depend on the size of the local region. Thus, by extending the local region corresponding to the first shell up to the second one, we see a significant increase of $\tau_{\Delta\rho_l}$ for all the investigated state points. These observations for sc CO_2 are in agreement with previous MD results on 2D pure LJ monatomic fluid model (see Fig. 3 in Ref. 30).

TABLE III. Parameter values c, t_1, and t_2 obtained from the fits of the model function of Eq. (7) to the simulated $C_{\Delta\rho l}(t)$ data at each investigated state point and for the first coordination shell of sc CO_2 and sc MeOH.

System	sc CO_2			sc MeOH		
State points	First shell			First shell		
	c	t_1	t_2	c	t_1	t_2
A	0.695	0.903	4.647	0.664	0.729	6.162
B	0.636	0.891	3.576	0.662	0.774	5.166
C	0.608	0.891	3.887	0.597	0.712	3.760
D	0.670	0.920	4.247	0.653	0.700	3.320
E	0.735	0.864	5.056	0.627	0.619	2.919
F	0.723	0.785	4.295	0.714	0.636	3.003
G	0.734	0.677	3.458	0.719	0.555	2.660
H	0.752	0.595	3.123	0.723	0.510	2.159
I	0.892	0.404	2.844	0.932	0.420	2.664

Moreover, to support further our findings that the relaxation of the local density around each particle in the first shell is a two time-scale dynamical process, we calculated the contribution of $C_1(t)$ and $C_2(t)$ to the total relaxation time $\tau_{\Delta\rho_l}$. From Eqs. (4) and (7), the local density reorganization time $\tau_{\Delta\rho_l}$ can be expressed by the following relation:

$$\tau_{\Delta\rho_l} = c \cdot t_1 + (1-c) \cdot t_2 = \tau_1 + \tau_2. \tag{8}$$

As we can see, the time $\tau_{\Delta\rho_l}$ is the sum of two different relaxation times τ_1 and τ_2. Figure 7(a) shows the density dependence of the relaxation times $\tau_{\Delta\rho_l}$, τ_1, and τ_2. From this figure we may observe that τ_1 are significantly smaller than τ_2 for low densities and up to $1.2\rho_c$. At this density region the τ_2 values are about two times greater than the τ_1 ones. In the high-density region, τ_2 decreases monotonically with density, while τ_1 remains almost constant in the whole density range. Finally, the density dependence of $\tau_{\Delta\rho_l}$ for the first shell from Figs. 4(c) and 7(a) shows a similar trend observed and discussed above for the relaxation time τ_2.

Interestingly, Yamaguchi *et al.*[48] performed simulations to investigate the nonpolar solvation dynamics in simple sc solvents and especially the effect of attractive and repulsive interactions between solute and solvent on the solvation processes. It is pointed out from that study that the solvation acf is divided into the short- and long-time parts. Moreover, the long-time behavior reflects mainly the effect of attractive interactions on solvation dynamics and is clearly density dependent, whereas the short time (initial) part of this relaxation procedure is almost density independent. So, such a behavior of the solvation acf seems to be quite similar to the behavior of the local density acf $C_{\Delta\rho_l}(t)$ of the first shell in our study.

Concerning the density dependence of $\tau_{\Delta\rho_l}$ for the second shell from Fig. 5(c), we can clearly see that it exhibits an increasing behavior in the low-density region and up to $1.2\rho_c$. At higher densities, $\tau_{\Delta\rho_l}$ decreases significantly with density as in the case of the first shell dynamics. A similar behavior has been observed for the 2D LJ monatomic model fluids as the radius of the coordination shell increases[30] and might be explained by the fact that in the density region close to the critical one the long-range fluctuations are maximized, causing the increase of $\tau_{\Delta\rho_l}$. Such a behavior signifies that a coupling between the dynamics of the local and extended structures exists and the long-range "critical slowing

TABLE IV. The calculated local environment lifetimes $\tau_{\Delta\rho l}$ for the first and second coordination shell of sc CO_2 and MeOH as a function of the reduced bulk density at $T/T_c = 1.03$, from this work.

Thermodynamic state points		sc CO_2 $\tau_{\Delta\rho l}$ (ps)		sc MeOH $\tau_{\Delta\rho l}$ (ps)	
Index	ρ/ρ_c	First shell	Second shell	First shell	Second shell
A	0.1903	2.031	2.452	2.576	2.240
B	0.3529	1.859	2.543	2.298	2.610
C	0.6095	2.055	3.083	1.964	2.650
D	0.8597	2.019	3.236	1.511	2.300
E	1.1441	1.955	3.089	1.486	2.310
F	1.2660	1.766	3.062	1.318	2.210
G	1.4329	1.422	2.499	1.170	1.920
H	1.5654	1.238	2.196	0.950	1.510
I	2.0000	0.679	1.122	0.564	0.830

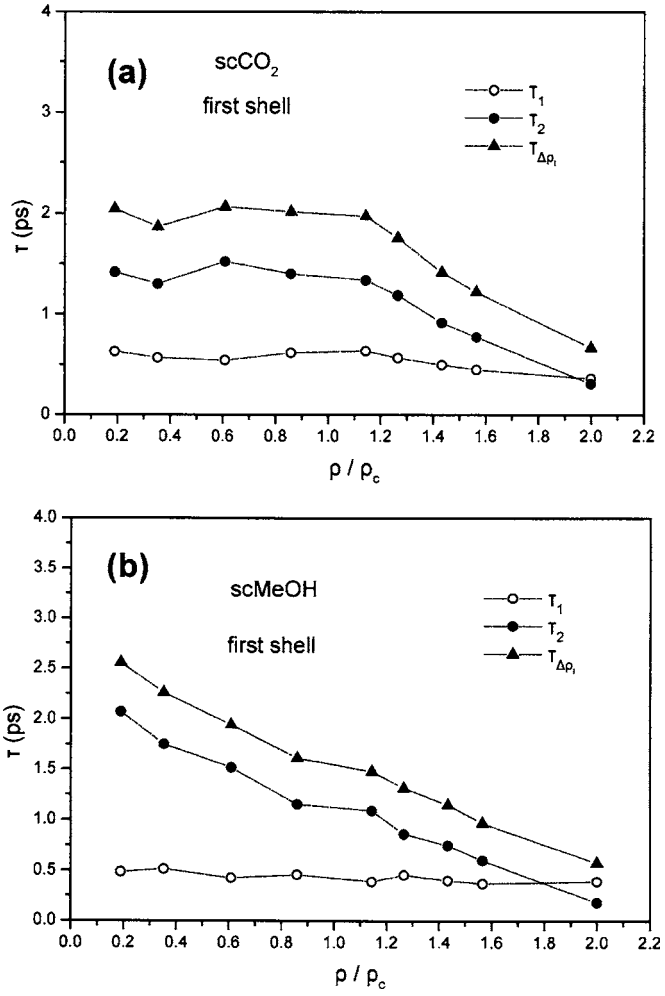

FIG. 7. (a) Density dependence of the calculated total local density reorganization time $\tau_{\Delta\rho_l}$ and its two components τ_1 and τ_2 for the first shell of molecules in sc CO_2. (b) Same as in (a), but for the first shell of sc MeOH.

down" effect affects the local density dynamics at larger length scales, as it has been also pointed out by Maddox *et al.*[30]

Concretely, the authors in that study proposed two different mechanistic sources for the creation of these local density inhomogeneities. The first one, named "potential induced" (or structural) occurs at short length scales, which are in the range of the direct intermolecular interactions. The contribution of this mechanism on the local structural effects at relatively low bulk densities seems to be quite important. The second one ("inhomogeneity induced") results from indirect intermolecular interactions at more extended length scales. Of course, such interactions are related to collective relaxation processes, and they are maximized near the critical density. To support further these arguments, we have to mention that Saitow *et al.* reported recent results concerning the time evolution of the density fluctuations in some hydrogen- and non-hydrogen-bonded scfs in a mesoscopic length scale by using dynamic light scattering techniques.[49,50] In that studies the authors investigated the dynamic behavior of the mesoscopic density fluctuations, and according to their results the relaxation times obtained exhibit maximum values near the critical density. Thus, we may conclude from our results of sc CO_2 that by increasing the radius R_c taken into account for the calculation of the local environment lifetimes of the second coordination shell, the density dependence of $\tau_{\Delta\rho_l}$ starts exhibiting a similar behavior as in the case for a mesoscopic length scale recorded experimentally.

2. sc MeOH

The acfs $C_{\Delta\rho_l}(t)$ of sc MeOH are presented in Figs. 4(b) and 5(b). From the curves in these figures we see that the time required for $C_{\Delta\rho_l}(t)$ approaching zero value decreases significantly with increasing density (from states A–I). For instance, from the curves in Fig. 4(b) we see that $C_{\Delta\rho_l}(t)$ at state A decays to zero after approximately 20 ps, while at state I (the highest density studied) after $\cong$10 ps. Further, a characteristic feature apparent in both Figs. 4(b) and 5(b) is that the time evolution of these correlations for both shells changes remarkably by increasing the density, as in the case of sc CO_2.

As in the case of sc CO_2, we found that $C_{\Delta\rho_l}(t)$ for sc MeOH cannot be fitted with one single exponential-type decay model function. The time evolution of these acfs for the first shell exhibits two different time-scale relaxation mechanisms that are more apparent in the high-density region, and the best-fit results were obtained with the function given by Eq. (7). In the case of the second shell, the acfs $C_{\Delta\rho_l}(t)$ could not be well fitted with the aforementioned model function.

Figure 8 presents the results from the fit procedure for the first shell, where the analysis of $C_{\Delta\rho_l}(t)$ in two component functions for some state points (states A, E, and I) is shown. The parameter values c, t_1, and t_2 are summarized in Table III.

From Fig. 8 and Table III, we can easily see that also in the case of sc MeOH the acf $C_1(t)$ contributes mainly to the shape of $C_{\Delta\rho_l}(t)$ at relatively small time scales and decays to zero quite fast, whereas $C_2(t)$ contributes at larger time scales and decays to zero quite slower than $C_1(t)$. Summing up, it is found that the dynamics of the first shell redistribution in both fluids is a two time-scale relaxation process. We may also observe from Fig. 8 that by increasing the bulk density, especially in the density range $1.2\rho_c$–$2.0\rho_c$ both acfs decay to zero faster. In the whole density range the values of $C_1(0)$ are significantly larger than the corresponding $C_2(0)$ ones. In the high-density region the values of $C_1(0)$ increase with density, while the values of $C_2(0)$ exhibit an opposite behavior and decrease more rapidly than even in the case of sc CO_2. This finding indicates that the contribution of the slow relaxation processes in the local environment reorganization mechanism of sc MeOH becomes very weak at higher densities.

The corresponding correlation times $\tau_{\Delta\rho_l}$ against density are plotted in Figs. 4(c) and 5(c) and depicted in Table IV. We may generally observe here that the density dependence of $\tau_{\Delta\rho_l}$ for the first shell exhibits a decreasing behavior by increasing density. Moreover, for densities greater than $1.2\rho_c$ the decrease of $\tau_{\Delta\rho_l}$ appears to be even larger. Another point of interest is the small plateau behavior of $\tau_{\Delta\rho_l}$ with density observed for densities in the region $0.8\rho_c$–$1.2\rho_c$. Note also

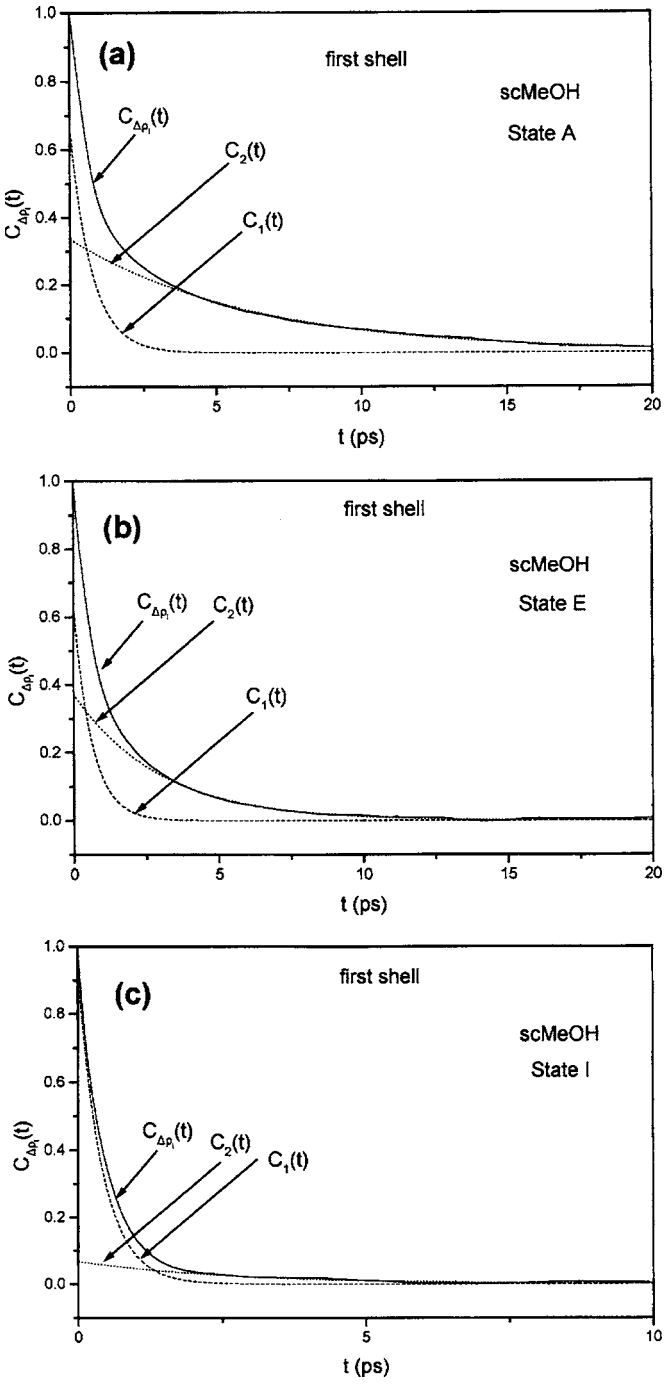

FIG. 8. Same as in Fig. 6 but for the first shell of molecules in sc MeOH.

that the times $\tau_{\Delta\rho_l}$ depend on the length of the local region. Thus, for the second shell an increase of $\tau_{\Delta\rho_l}$ in comparison with those of the first shell is observed, as in the case of sc CO_2.

Summing up, it seems clearly that the density dependence of the first shell local density lifetimes $\tau_{\Delta\rho_l}$ of sc MeOH is sufficiently different from those of sc CO_2. We found, however, that this behavior is quite similar to that of the local density dynamics in sc water (scw), as our MD simulations of this fluid[51] have newly revealed. In scw, where it has been found that the existence of strong augmentation effects is even more pronounced[51] in comparison with sc CO_2 and sc MeOH, the correlation times $\tau_{\Delta\rho_l}$ for the first shell exhibit a decreasing behavior by increasing density. This similarity for the HB scfs MeOH and water is probably related to the increase of the collisional events among the hydrogen-bonded molecules, leading to a more frequent breaking of hydrogen bonds and eventually to a faster local density reorganization process at the region of high density.

For the second shell [see Fig. 5(c)], the behavior of $\tau_{\Delta\rho_l}$ against density provides similarities with those of sc CO_2. So, at low densities $\tau_{\Delta\rho_l}$ exhibits an increase followed by a significant decrease. Finally, it seems that the density dependence of $\tau_{\Delta\rho_l}$ for the second shell dynamics of sc MeOH may be attributed to the aforementioned features we have already mentioned above to explain the similar behavior of sc CO_2.

The contributions of $C_1(t)$ and $C_2(t)$ in the total relaxation time $\tau_{\Delta\rho_l}$, reflected by the correlation times τ_1 and τ_2 are in Fig. 7(b). From this figure we may observe that at low densities and up to $1.2\rho_c$ the times τ_2 are about three to four times greater than the τ_1 ones. In addition, in the high-density region τ_2 decreases rapidly while τ_1 remains almost constant with density. Finally, at liquidlike densities $(2.0\rho_c)$ the contribution of τ_2 on is very small. Interestingly, we found that this different behavior between τ_1 and τ_2 with density in sc MeOH is similar to that obtained for sc CO_2 and scw (not presented in Ref. 51). This effect could be related to the different contributions of the intermolecular interactions to the fast and slow local density reorganization processes which, as it has been shown above [see Eq. (7) and Fig. 6], are revealed by the time decay of $C_1(t)$ and $C_2(t)$, respectively.

According to the suggestion of Maddox *et al.*,[30] the more significant contribution of the slow part $C_2(t)$ to $C_{\Delta\rho_l}(t)$ may be attributed to the attractive interactions among the molecules which, especially at low and intermediate densities lead to the formation of small metastable clusters that dissociate only rarely. Note, however, that at high densities the contribution of the attractive interactions in determining the local density reorganization of the first shell, characterized as potential induced mechanism,[30] could not be the underlying one as it is indirectly shown from the time decay of $C_2(t)$ with density. On the other hand, the correlation time $\tau_1 = C_1(0) \cdot t_1 = c \cdot t_1$ has been found to be independent of the density and is presumably determined by the short-range repulsive part of the intermolecular potential.

We recall to this point that the static (zero-time) value $C_1(0)$ (see Figs. 6 and 8 and Table III) exhibits an increasing behavior more pronounced at higher densities. This effect may be characterized as a consequence of the very short-range local structure alteration at higher densities. This fact is in agreement with the statement that at liquidlike densities the short-range local structure is mainly determined by the repulsive interactions.[52]

Contrary to the behavior of $C_1(0), C_1(t)$ decays faster with density, and that leads to a systematic decrease of t_1 with density. The more rapid decrease of $C_1(t)$ at high densities is presumably related to the decrease of the binary collision time among the particles in the fluid. Therefore although $C_1(0)$ increases and t_1 decreases with density the product $C_1(0) \cdot t_1 = c \cdot t_1 = \tau_1$ [see Eqs. (7) and (8)] remains virtually constant.

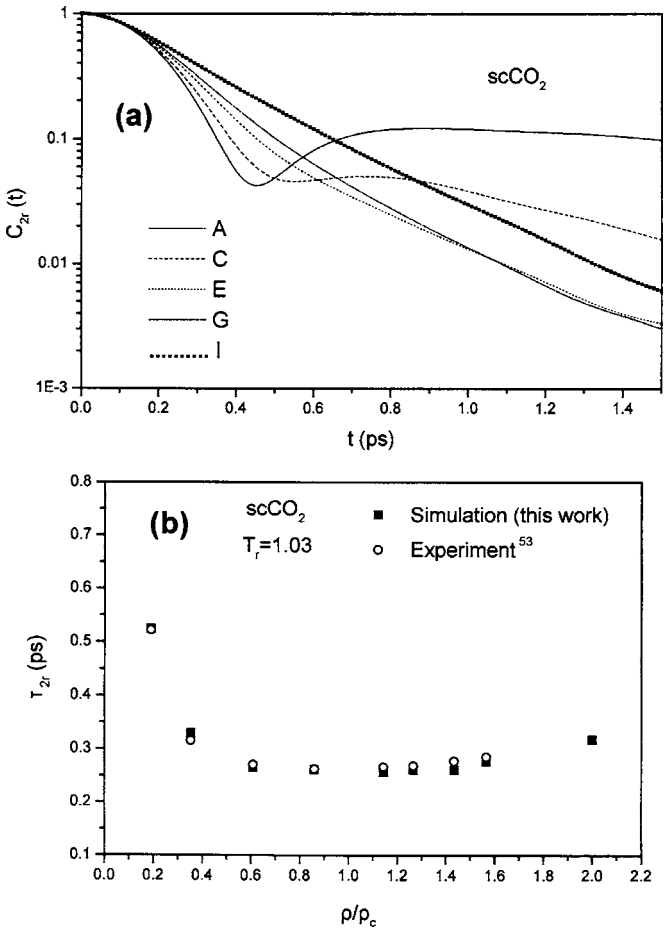

FIG. 9. (a) Semilogarithmic plot of the calculated second-order Legendre reorientational acfs $C_{2r}(t)$ of sc CO_2. (b) Bulk density dependence of the calculated reorientational correlation time τ_{2r} of sc CO_2, in comparison with experiment (Ref. 53).

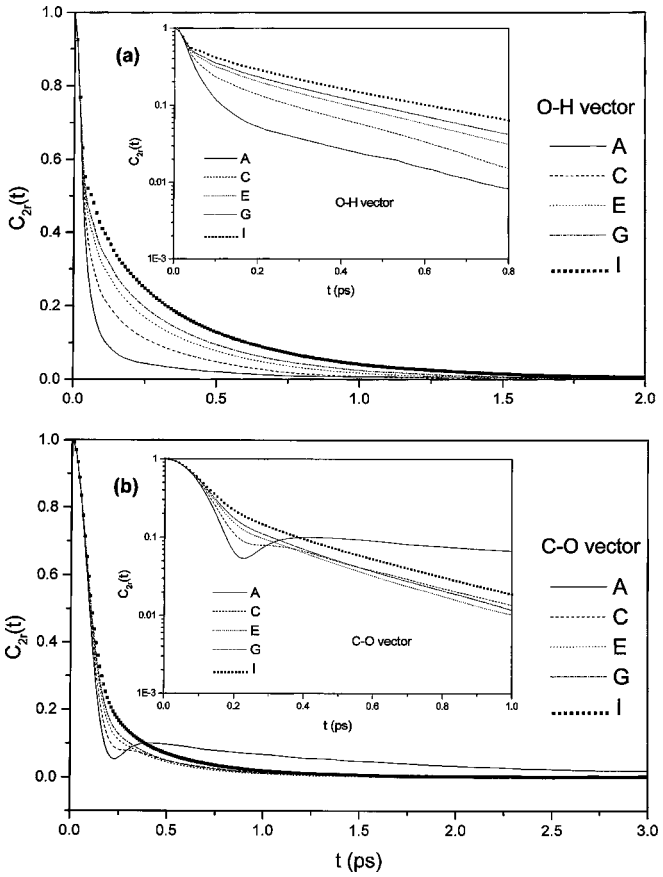

FIG. 10. The calculated second-order Legendre reorientational acfs $C_{2r}(t)$ for (a) the unit vector on the O–H bond and (b) the unit vector on the C–O bond of sc MeOH. In the inset pictures the semilogarithmic plots of $C_{2r}(t)$ are also presented.

C. Reorientational dynamics

In this section, we will report on our results concerning the single-molecule reorientational dynamics of both scfs. Their density dependence will also be discussed in detail with corresponding local environment static and dynamical effects mentioned before. The main purpose of this part is to seek for a possible interrelation between the single-molecule dynamics and the local environment ones.

The single reorientational dynamics of the fluids were investigated as usual by means of the Legendre acfs. In the case of CO_2, we have used a unit vector along the C–O axis, whereas for MeOH the unit vectors we have used that along the C–O and O–H axes. The Legendre reorientational acfs are defined by the well-known relation

$$C_{lr}(t) = \langle P_l(\vec{u}(0) \cdot \vec{u}(t)) \rangle, \quad l = 1,2. \tag{9}$$

The corresponding second order Legendre reorientational acfs for the CO_2 and MeOH molecules are depicted in Figs. 9(a), 10(a), and 10(b), respectively.

The reorientational correlation times τ_{2r} for CO_2 and MeOH have been evaluated by integrating the corresponding normalized acfs, and the results are presented in Figs. 9(b) and 11, respectively. The times τ_{2r} for CO_2 have been compared with results from NMR measurements of the fluid[53] at exactly the same state points. As we can clearly see from Fig. 9, the agreement between experiment and simulation is very good. Furthermore, we see that at low densities τ_{2r} exhibits a rapidly decreasing behavior with density up to about $0.6\rho_c$. For densities between $0.6\rho_c$ and $1.4\rho_c$, the time τ_{2r} reveals a plateau behavior followed by a slightly increasing one, which takes place in the highest density region. The aforementioned plateau behavior has been also observed by

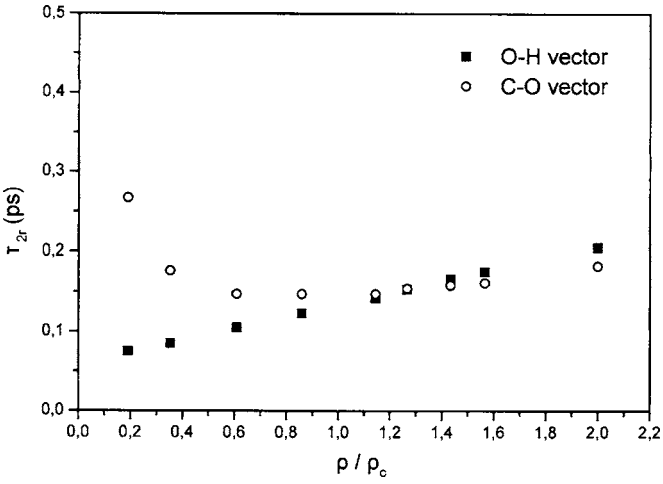

FIG. 11. Density dependence of the calculated reorientational correlation time τ_{2r} for the O–H and C–O unit vectors of molecules in sc MeOH.

Umecky *et al.*[53] and Holz *et al.*[54] in their NMR measurements of pure sc CO_2 at the slightly higher temperature $T=319$ K. Also, a similar behavior has been observed from a previous MD simulation of the neat fluid at $T=307$ K (Ref. 38) and $T=323$ K.[55]

Before proceeding any further, it is very important to pay some attention to the shape of the calculated Legendre acfs of sc CO_2. According to previous simulation[38] and experimental[53,54] studies, the reorientational dynamics of sc CO_2 might be considered as diffusive only at the high-density region. By inspecting our results in Fig. 9(a) we can clearly see that the time decay of $C_{2r}(t)$ of sc CO_2 exhibits clear density dependence. We may also observe that the decay of these acfs could be fitted by single exponential decay functions only at the density region above $1.4\rho_c$. At this density region, where the reorientational motion of the molecules could be considered as a diffusive one, the behavior of τ_{2r} against density is quite similar to that observed at liquidlike conditions.

Generally, we may observe that as the bulk density increases the reorientational relaxation mechanism changes from a gaslike (free-rotor-like) one to a liquidlike diffusive one. We may also notice that the switch from the gaslike to the liquidlike behavior takes place at the range of densities close to the critical one. At very low densities the fluid is mainly consisted of molecules that rotate quite freely, but also of a fraction of molecules that form small metastable clusters.[30] However, at intermediate densities close to ρ_c, due to the existence of strong local density augmentation effects the local environment around each molecule is more cohesive, leading thus to a more constrained reorientational motion. Presumably, this is the reason why the switch of the relaxation mechanism, which is reflected in the change of the time decay of $C_{2r}(t)$, is observed in this density region. Furthermore, the characteristic changes in the static and dynamic behaviors of the local environment in the intermediate density region close to ρ_c seem to affect very slightly the values of τ_{2r}, causing thus this plateau behavior in this specific density region.

A similar behavior has been also revealed from the results obtained by using Raman measurements and MD simulations of sc CHF_3.[56] Note also that Zerda *et al.*[57] investigated further the role of angular velocity acf and its appearance to rotational relaxation dynamics from the low- to the high-density region in the case of sc SF_6.

Another interesting feature here is that the increase of τ_{2r} with density is observed at the density region where the local density augmentation values, as well as the $\tau_{\Delta\rho_l}$ ones, start exhibiting a rapid decreasing behavior. In other words, at the density region where the local density reorganization processes become faster, the single-molecule reorientational relaxation processes start to become slightly slower. Additionally, from Figs. 2(c) and 9 the curves of the local enhancement factors versus density exhibit an inflection point at the density where τ_{2r} starts increasing ($\sim 1.2\rho_c$).

These observations could be indications that the single-molecule dynamics might be affected by the local density inhomogeneities and their time dependent behavior. A similar feature has been also pointed out by Cabaco *et al.*[58] in a recent spectroscopic experimental study of the rotational relaxation of sc hexafluorobenzene. However, all the above considerations lead to qualitative conclusions, and probably the use of pure analytical theoretical models might be required in order to investigate these effects from a more quantitative point of view.

The C–O and O–H reorientational dynamics of sc MeOH were investigated separately in order to explore the sensitivity of these specific reorientational motions to the local environment around each molecule. From Figs. 10(a) and 10(b) we can see that the reorientational motion of the C–O unit vector is quite different from that of the O–H one in the whole density range. This behavior has been also revealed from a very recent CS study of our group concerning the reorientational dynamics of sc EtOH.[59] The reorientational motion of the C–O bond vector of MeOH at low densities is sufficiently more hindered than the corresponding one of the O–H vector. By inspecting the time evolution of the C–O second order reorientational acf at the lowest density (state A), we observe a very rapid decay until $t=0.25$ ps. At this time the acf exhibits a local positive minimum. In the time interval of 0.25–0.4 ps the acf increases and exhibits a local maximum at $t=0.4$ ps, followed by an almost exponentially slow decay. As the density becomes greater, the aforementioned behavior changes and for densities higher than $1.2\rho_c$ the reorientational motion of both vectors exhibits a clearer diffusive behavior, as we can see from the semilogarithmic plot of $C_{2r}(t)$ [see inset picture in Fig. 10(b)].

Moreover, the density dependence of τ_{2r} in the case of C–O is presented in Fig. 11. It is seen from this figure that at low densities τ_{2r} exhibits a rapidly decreasing behavior up to $0.6\rho_c$. For densities in the range of $0.6\rho_c-1.4\rho_c$, τ_{2r} remains almost constant, and in the highest density region ($>1.2\rho_c$) it exhibits a slightly increasing behavior with density. Interestingly, this behavior is found to be very similar to that of τ_{2r} in the case of sc CO_2. To our knowledge, experimental results concerning the particularly interesting behavior of the C–O reorientational dynamics with density in liquid as well as in sc MeOH have never been published so far. In a recent experimental study, Yamaguchi *et al.*[60] published results for the O–H reorientational dynamics of sc MeOH at 543 K. Therefore, at this stage the simulated C–O dynamics of sc MeOH cannot be compared with experiment.

The O–H $C_{2r}(t)$ acfs are shown in Fig. 10(a), and as we can see they are quite different from those corresponding to the C–O vector. As the density increases the decay of the O–H acf becomes slower. Thus, at the lowest density (state A) the time required for $C_{2r}(t)$ to approach zero is about 1 ps, while at the highest one it is about 2 ps. Note also that from the semilogarithmic plot of $C_{2r}(t)$ [see inset picture in Fig. 10(a)] we can see that only at the high-density region ($1.4\rho_c-2.0\rho_c$) the shape of this correlation is quite similar to that of an exponential decay function and thus the reorientational motion of the O–H vector might be characterized as a diffusivelike one.

The density dependence of τ_{2r} in the case of the O–H vector was investigated, and the results are shown in Fig. 11. In contrast to the C–O results, the time τ_{2r} exhibits an in-

creasing behavior with density in the whole investigated range. This behavior is quite similar compared to the results of Yamaguchi *et al.*[60] Also, the simulated and experimental values of τ_{2r} have been found in quite good agreement, regardless of the experimental data corresponding to a somewhat higher temperature than the simulated ones.

Finally, the τ_{2r} behavior obtained might be explained by taking into account the fact that as the system density increases the HB network around the methanol molecules becomes stronger,[41] making the reorientational motion of the O–H vector quite slower. The sensitivity of the O–H reorientational dynamics to the microscopic HB interactions in self-associated fluids has also been revealed from previous studies of our group concerning the reorientational dynamics of sc ethanol,[59] where a similar behavior has been also observed. At lower bulk densities the reorientational correlation times obtained are quite smaller due to the collapse of the HB network, a result suggested by previous simulation studies[41,59] and NMR experimental studies.[29]

IV. CONCLUSIONS

The molecular dynamics simulation technique was used to investigate the features concerning the LDIs and their dynamics in sc CO_2 and MeOH. The simulations were carried out along near critical isotherms and for densities below and above the critical one. The methodology employed to estimate the properties related to the inhomogeneities present in each fluid was based on the calculation of the excess local density (augmentation) relative to the bulk one, $\Delta\rho_{\mathrm{eff}_2 l}$, as well as the well-known enhancement factor F_{enh}. The time evolution of the local density redistribution in both scfs was studied in terms of the instantaneous local density deviation relative to the mean local acfs, $C_{\Delta\rho_l}(t)$, and the corresponding correlation time $\tau_{\Delta\rho_l}$. We found that the local density augmentation in sc MeOH is sufficiently stronger in comparison with sc CO_2, which might be attributed to the compact hydrogen-bonding associative character of MeOH. For both fluids, the local density augmentation is maximized in the density region close to $0.7\rho_c$ and exhibits a clear decrease from the first to the second solvation shell.

The shape and time decay to zero of $C_{\Delta\rho_l}(t)$ changes significantly from low to high densities for both shells, signifying the density effect upon the dynamics of the local density redistribution. We found that for both scfs a sum of two exponential decay functions might be proposed as the most suitable one for the description of the characteristic features of the first shell redistribution dynamics. Thus, the correlation time $\tau_{\Delta\rho_l}$ could be expressed as the sum of two different correlation times τ_1 and τ_2 [Eq. (8)]. This behavior is more pronounced especially in the low-density region up to $1.2\rho_c$. Our findings indicate for the first time that the description of the dynamical behavior of the local density redistribution around each molecule at short length scales (first shell) involves two relaxation processes, namely, one responsible for the short-time dynamics and the other one describing the long-time behavior.

The density dependence of $\tau_{\Delta\rho_l}$ for the first shell in sc MeOH is sufficiently different from that of sc CO_2. We also found that in both systems the correlation times τ_1 are significantly smaller than the τ_2 ones for low densities up to $1.2\rho_c$. In the high-density region, τ_2 decreases rapidly with density, while τ_1 remains virtually constant in the whole density range.

Contrary to the time evolution of $C_{\Delta\rho_l}(t)$ for the first shell, the local density redistribution dynamics for the second one could not be interpreted in terms of a sum of two exponential decay model functions. This result indicates that by increasing the length scale of the local region the overall responsible mechanism for the relaxation of the corresponding environment around a tagged molecule becomes more complicated.

The $\tau_{\Delta\rho_l}$ values obtained for the second shell exhibit an increasing behavior at low densities and are maximized in the density region close to the critical one. Also, as in the case of the first shell, they decrease significantly at higher densities.

To explore for a possible interrelation between the single-molecule and local environment dynamics, the single reorientational dynamics of the molecules in both systems were investigated by means of the Legendre acfs. The reorientational motion of the C–O unit vector in sc MeOH is found to be very different from that of O–H in the whole density range studied. Especially at low densities, the C–O dynamics are much more hindered than the corresponding O–H ones. Note that the O–H relaxation time τ_{2r} exhibits an increasing behavior with density. Such a behavior might be attributed to the HB network around the methanol molecules. With regard to the relaxation time τ_{2r} for C–O, the results obtained predict clearly a plateau for densities in the range $0.6\rho_c-1.4\rho_c$. A similar plateau behavior of the calculated τ_{2r} values was clearly observed in the case of sc CO_2. This finding could be probably related with the fact that the local density augmentation values and the corresponding local density reorganization times are maximized in the bulk density region where this plateau is observed, indicating the existence of an interrelation between the single-molecule and local environment dynamics. However, a further systematic investigation of the role of HB interactions to the static and dynamic behavior of LDIs and their interrelation with single dynamic properties in associated fluids is needed and eventually remains one of our further goals in this field of investigation.

ACKNOWLEDGMENTS

The authors are grateful to Dr. M. Kanakubo (National Institute of Advanced Industrial Science and Technology 4-2-1 Nigatake, Miyagino-ku, Sendai 983-8551, Japan) for sending us his experimental reorientational correlation times of sc CO_2 and Dr. Dietmar Paschek (University of Dortmund, Germany) for useful comments and discussion on specific computational aspects. The CPU time allocation on the facilities of the Computing Center of the University of Athens-Greece is also gratefully acknowledged. This work was supported by the National University of Athens-Greece Grant No. 70/4/6485.

[1] S. C. Tucker, Chem. Rev. (Washington, D.C.) **99**, 391 (1999).
[2] S. C. Tucker and M. W. Maddox, J. Phys. Chem. B **102**, 2437 (1999).
[3] G. Goodyear, M. W. Maddox, and S. C. Tucker, J. Chem. Phys. **112**, 10327 (2000).
[4] G. Goodyear, M. W. Maddox, and S. C. Tucker, J. Phys. Chem. B **104**, 6240 (2000).
[5] M. W. Maddox, G. Goodyear, and S. C. Tucker, J. Phys. Chem. B **104**, 6248 (2000).
[6] O. Kajimoto, Chem. Rev. (Washington, D.C.) **99**, 355 (1999).
[7] W. Song, R. Biswas, and M. Maroncelli, J. Phys. Chem. A **104**, 6924 (2000).
[8] J. Lewis, R. Biswas, A. Robinson, and M. Maroncelli, J. Phys. Chem. B **105**, 3306 (2001).
[9] T. Aizawa, M. Kanakubo, Y. Ikushima, R. L. Smith Jr., T. Saitoh, and N. Sugimoto, Chem. Phys. Lett. **393**, 31 (2004).
[10] M. Okamoto, H. Nagashima, and F. Tanaka, Phys. Chem. Chem. Phys. **4**, 5627 (2002).
[11] J. K. Rice, E. D. Niemeyer, R. A. Dunbar, and F. V. Bright, J. Am. Chem. Soc. **117**, 5830 (1995).
[12] B. L. Knutson, D. L. Tomasko, C. A. Eckert, P. G. Debenedetti, and A. A. Chialvo, in *Supercritical Fluid Technology*, ACS Symposium Series Vol. 488, edited by F. V. Bright and M. E. McNally (American Chemical Society, Washington, DC, 1992), pp. 60–72.
[13] S. Egorov, J. Chem. Phys. **112**, 7138 (2000).
[14] N. Patel, R. Biswas, and M. Maroncelli, J. Phys. Chem. B **106**, 7096 (2002).
[15] A. Siavosh-Haghighi and J. E. Adams, J. Phys. Chem. A **105**, 2680 (2001).
[16] S. A. Egorov, A. Yethiraj, and J. L. Skinner, Chem. Phys. Lett. **317**, 558 (2000).
[17] I. B. Petsche and P. G. Debenedetti, J. Chem. Phys. **91**, 7075 (1989).
[18] F. W. Favero and M. S. Skaf, J. Supercrit. Fluids **34**, 237 (2005).
[19] M. Echargui and F. Marsault-Herail, Mol. Phys. **60**, 605 (1987).
[20] D. Ben-Amotz, F. LaPlant, D. Shea, J. Gardecki, and D. List, in *Supercritical Fluid Technology*, ACS Symposium Series Vol. 488, edited by F. V. Bright and M. E. McNally (American Chemical Society, Washington, DC, 1992), pp. 18–30.
[21] H. Nakayama, K. Saitow, M. Nakashita, K. Ishii, and K. Nishikawa, Chem. Phys. Lett. **320**, 323 (2000).
[22] M. I. Cabaco, M. Besnard, T. Tassaing, and Y. Danten, Pure Appl. Chem. **76**, 141 (2004).
[23] W. Song and M. Maroncelli, Chem. Phys. Lett. **378**, 410 (2003).
[24] S. A. Egorov, Chem. Phys. Lett. **354**, 140 (2002).
[25] K. Saitow, H. Ohtake, N. Sarukura, and K. Nishikawa, Chem. Phys. Lett. **341**, 86 (2001).
[26] K. Saitow, K. Otake, H. Nakayama, K. Ishii, and K. Nishikawa, Chem. Phys. Lett. **368**, 209 (2003).
[27] K. Saitow, H. Nakayama, K. Ishii, and K. Nishikawa, J. Phys. Chem. A **108**, 5770 (2004).
[28] K. Saitow and J. Sasaki, J. Chem. Phys. **112**, 104502 (2005).
[29] M. M. Hoffmann and M. S. Conradi, J. Phys. Chem. B **102**, 263 (1998).
[30] M. W. Maddox, G. Goodyear, and S. C. Tucker, J. Phys. Chem. B **104**, 6266 (2000).
[31] F. Marsault-Herail and M. Echargui, J. Mol. Liq. **48**, 211 (1991).
[32] H. J. C. Berendsen, J. P. M. Postma, W. F. van Gunsteren, A. DiNola, and J. R. Haak, J. Chem. Phys. **81**, 3684 (1984).
[33] J. P. Ryckaert, G. Ciccotti, and H. J. C. Berendsen, J. Comput. Phys. **23**, 327 (1977).
[34] M. P. Allen and D. J. Tildesley, *Computer Simulation of Liquids* (Oxford University Press, Oxford, UK, 1987).
[35] D. Paschek and A. Geiger, MOSCITO 4.1, University of Dortmund, Dortmund, Germany, 2003.
[36] J. G. Harris and K. H. Young, J. Phys. Chem. **99**, 12021 (1995).
[37] W. L. Jorgensen, J. Chem. Phys. **90**, 1276 (1986).
[38] J. E. Adams and A. Siavosh-Haghighi, J. Phys. Chem. B **106**, 7973 (2002).
[39] M. Saharay and S. Balasubramanian, J. Chem. Phys. **120**, 9694 (2004).
[40] N. Asahi and Y. Nakamura, J. Chem. Phys. **109**, 9879 (1998).
[41] M. Chalaris and J. Samios, J. Phys. Chem. B **103**, 1161 (1999).
[42] M. Chalaris and J. Samios, Pure Appl. Chem. **76**, 203 (2004).
[43] G. Chatzis and J. Samios, Chem. Phys. Lett. **374**, 187 (2003).
[44] S. R. P. da Rocha, K. P. Johnston, R. E. Westacott, and P. J. Rossky, J. Phys. Chem. B **105**, 12092 (2001).
[45] I. Skarmoutsos and J. Samios, J. Mol. Liq. **125**, 181 (2006).
[46] S. Chappini, M. Nardone, F. P. Ricci, and M. C. Bellissent-Funel, Mol. Phys. **89**, 975 (1996).
[47] S. Nugent and B. M. Ladanyi, J. Chem. Phys. **120**, 874 (2004).
[48] T. Yamaguchi, Y. Kimura, and N. Hirota, J. Chem. Phys. **111**, 4169 (1999).
[49] K. Saitow, D. Kajiya, and K. Nishikawa, J. Phys. Chem. A **109**, 83 (2005).
[50] K. Saitow, D. Kajiya, and K. Nishikawa, J. Phys. Chem. A **109**, 7365 (2005).
[51] I. Skarmoutsos and J. Samios, J. Phys. Chem. B **110**, 21931 (2006).
[52] J. D. Weeks, D. Chandler, and H. C. Andersen, J. Chem. Phys. **54**, 5237 (1971).
[53] T. Umecky, M. Kanakubo, and Y. Ikushima, J. Phys. Chem. B **107**, 12003 (2003).
[54] M. Holz, R. Haselmeier, A. J. Dyson, and H. Huber, Phys. Chem. Chem. Phys. **2**, 1717 (2000).
[55] K. Kiyohara, Y. Kimura, Y. Takebayashi, N. Hirota, and K. Ohta, J. Chem. Phys. **117**, 9867 (2002).
[56] S. Okazaki, M. Matsumoto, I. Okada, K. Maeda, and Y. Kataoka, J. Chem. Phys. **103**, 8594 (1995).
[57] T. W. Zerda, J. Schroeder, and J. Jonas, J. Chem. Phys. **75**, 1612 (1981).
[58] M. I. Cabaco, M. Besnard, T. Tassaing, and Y. Danten, J. Mol. Liq. **100**, 181 (2006).
[59] D. Dellis, M. Chalaris, and J. Samios, J. Phys. Chem. B **109**, 18575 (2005).
[60] T. Yamaguchi, N. Matubayasi, and M. Nakahara, J. Phys. Chem. A **108**, 1319 (2004).